Proton and neutron density distributions at supranormal density in low- and medium-energy heavy-ion collisions. II. Central Pb + Pb collisions

J. R. Stone
Department of Physics and Astronomy, University of Tennessee, Knoxville, Tennessee 37996, USA and Department of Physics (Astrophysics), University of Oxford, Oxford OX1 3RH, United Kingdom

P. Danielewicz
Facility for Rare Isotope Beams and Department of Physics and Astronomy, Michigan State University, East Lansing, Michigan 48824, USA

Y. Iwata
Faculty of International Studies, Osaka University of Economics and Law, Osaka 581-8511, Japan

(Received 13 August 2023; revised 30 November 2023; accepted 8 March 2024; published 1 April 2024)

This paper represents a continuation of our investigation into the limitations on total, proton, and neutron particle number densities, as well as the asymmetry of proton and neutron density distributions achievable in central heavy-ion collisions. We explore these aspects at low and medium energies within the framework of the Boltzmann-Uhlenbeck-Uehling (pBUU) transport and time-dependent Hartree-Fock (TDHF) models. Previous studies, focusing on symmetric and asymmetric collisions of Ca and Sn nuclei [1], and initial results on Pb-nuclei collisions [2], emphasized the role of the Coulomb interaction in these events. Our findings indicated that: (i) the highest total densities predicted at $E_{\rm beam} = 800$ MeV/nucleon were on the order of $\approx 2.5\rho_0$ ($\rho_0 = 0.16\,{\rm fm}^{-3}$), (ii) the proton-neutron asymmetry for maximal densities, $\delta = (\rho_{\rm n}^{\rm max} - \rho_{\rm p}^{\rm max})/(\rho_{\rm n}^{\rm max} + \rho_{\rm p}^{\rm max})$, did not generally exceed the asymmetry in the initial state of the collision at all beam energies and tended to decrease during the reaction, and (iii) a significant portion of this asymmetry had its microscopic origin in Coulomb forces, masking the pure nuclear contribution. These new findings, particularly relevant in the astrophysical context, are further examined in this work, focusing on the heaviest target-projectile combination ^{212,208}Pb accessible in an experiment. We introduce the SkT3 Skyrme force model, not previously used for the Pb system, and compare it to the SV-bas and SV-sym34 models to explore the symmetry-energy dependence of the results. Contour plots of nucleonic densities are presented, contrasting the time evolution of the density distributions in low (TDHF) and high (pBUU) models. We also present the evolution of normalized maximal proton, neutron, and total nucleon number density with increasing beam energy in the full pBUU model and the Vlasov approximation, aiming to explore the impact of correlations in the reaction. The time evolution of the proton and neutron density distributions in the plane transverse to the beam direction is illustrated at both low and high beam energy. In conclusion, our detailed examination of the Pb system in this work provides further essential evidence that the aforementioned findings (i)–(iii) are only weakly dependent on system size and a symmetry-energy model, and thus, they are of more general importance.

DOI: 10.1103/PhysRevC.109.044603

I. INTRODUCTION

In our previous work [1] (Paper I hereafter), we studied central heavy-ion collisions (HIC) of ^{40}Ca + ^{40}Ca, ^{40}Ca + ^{48}Ca, ^{48}Ca + ^{48}Ca, ^{100}Sn + ^{100}Sn, ^{100}Sn + ^{120}Sn, and ^{120}Sn + ^{120}Sn systems at nonrelativistic and moderately relativistic energies below 800 MeV/nucleon in the framework of the Boltzmann-Uhlenbeck-Uehling (pBUU) transport and time-dependent Hartree-Fock (TDHF) models.

The primary aim of those simulations was to determine limits on the total, proton, and neutron particle number densities and the asymmetry for proton and neutron density distributions that can be reached in HIC in this beam energy range. Somewhat unexpectedly, we found that the highest total densities predicted were of the order of $\approx 2.5\,\rho_0$ ($\rho_0 = 0.16\,{\rm fm}^{-3}$) and the proton-neutron asymmetry $\delta = (\rho_{\rm n}^{\rm max} - \rho_{\rm p}^{\rm max})/(\rho_{\rm n}^{\rm max} + \rho_{\rm p}^{\rm max})$ at maximum density was not exceeding, in the majority of cases, the asymmetry in the initial state of the collision and was generally decreasing in the reaction. Most surprising has been the significant role of the Coulomb force in the proton-neutron asymmetry, which led to a rapid publication of the first results [2].

However, despite the encouraging first indication [2], a detailed examination of system size dependence of reaction

dynamics is still lacking, limited to Ca and Sn. The present work on the asymmetric ^{212}Pb + ^{208}Pb (PB212208) system is designed to fill this gap.

The paper is organized as follows. The numerical methods and their physical basis and validity are explained in Sec. II. The results and discussion are presented in Sec. III. Conclusions and outlook form the content of Sec. IV.

II. CALCULATION METHOD

The same computational tools have been used in this work as in Paper I. The pBUU transport model simulated collision dynamics in the beam energy range $E_{\text{beam}} \leqslant 800$ MeV/nucleon. In addition, the TDHF technique was employed for low beam energy collisions at $E_{\text{beam}} \leqslant 40$ MeV/nucleon. The physical background of both models has been given in detail in Paper I. Here we remind the reader of only a few more general features of the calculations.

A. Computational strategy

As already stressed in Paper I, the initial state of a reaction plays an essential role in the simulation. For use in the pBUU framework, the static properties of the ground state of the target and projectile are obtained from a self-consistent solution of the Thomas-Fermi (TF) equations. This contrasts with the TDHF model, where the initial state is determined by a self-consistent solution of the Skyrme Hartree-Fock (SHF) equations in the three-dimensional (3D) geometry. However, both methods use minimization of the total energy density functional describing a spherical nucleus; the TF functional averages out shell effects while the SHF includes them fully.

Turning to the dynamics (time dependence) of the collisions, the difference between the pBUU and TDHF methods reflects the physics nature of the colliding system in the beam energy range where they are applied (for more discussion, see Sect. II B 2, Paper I and Ref. [3]). TDHF dynamics results from the solution of 3D time-dependent 3D Hartree-Fock equations fully including the shell effects [4]. At the same time, the pBUU framework follows a set of Boltzmann equations for nucleons, baryon resonances, and pions, solved using the test-particle Monte Carlo method, but leaving any shell effects out [5].

B. Validity considerations

1. Statistical fluctuations

As this work focuses on finding maximum particle densities over position and time, any statistical fluctuations in the Monte Carlo calculations outside the pBUU model framework may be of concern. We reiterate here that the simulation methods employed in this work are single-particle, potentially underestimating the role of fluctuations. At lower energies, the nature and magnitude of fluctuations are not well established. As we are interested in the maxima of statistically averaged densities reached during the compression stage of the collision, the fluctuations are short-lived and do not significantly affect the evolution of the averaged densities. Thus, single-particle approaches such as pBUU and TDHF are fully justified. To minimize possible effects of numerical fluctuations on deduced maxima, we use a relatively large number of test particles per physical particle in pBUU $\mathcal{N}_Q = 3000$.

2. Reaction mechanism at low and medium beam energy

At low beam energies, typically at incident energy up to about 40 MeV/nucleon, the HIC reaction mechanism differs from that assumed in the pBUU model. At energy sufficient to overcome the Coulomb barrier, the colliding system goes through two main phases: fusion and complete overlap of the target and projectile, followed by disintegration into two or more fragments. The nucleon mean-free path at low energies exceeds the size of the composite system. The TDHF theory, a nonperturbative approach that allows a description of a multinucleon transfer, is currently the best available framework, combining realism with flexibility and convenience in the low energy range (see, e.g., [6] in which the upper limit energy of TDHF is quantitatively shown).

This contrasts with strongly excited systems produced at higher beam energies, where the nucleon mean free path shrinks below the system size and decreases as the beam energy increases. With their statistical nature, the semiclassical pBUU or the molecular dynamics models [7,8] are the only practical approaches to studying collision at higher energies, with the omission of shell effects being less critical.

3. Particle flow

The mean-free path of particles in the HIC is closely related to the character of particle flow, and it is interesting to follow its changes with the incident beam energy. Surprisingly, the HIC flow can be viewed in terms of concepts from vacuum technology, for example, in particle accelerators or other devices relying on high vacuum [9]. Vacuum technology usually distinguishes three types of gas flow: viscous or continuum flow with closely interacting molecules, molecular flow with molecules moving freely without mutual interference, and a transitional range between viscous and molecular flow, known as Knudsen flow [10], arising where a molecule's free path length is similar to the size of the system.

In HIC at low energies, the mean-free path between elementary nucleon-nucleon collisions exceeds system size, the ensemble of nucleons follows the molecular flow, and the TDHF approach can grasp more physics than semi-classical transport represented by pBUU. At intermediate energies, the mean free path becomes shorter than the system size but is still comparable; the ensemble follows the so-called transitional flow, and the transport theory becomes necessary. Only at ultrarelativistic energies, with many new particles produced, does the mean-free path between elementary collisions become much shorter than the system size, the particle ensemble follows continuous flow, and hydrodynamics is called for. This work covers the upper end of the energy bracket for molecular flow and the lower end for transitional or Knudsen flow.

4. The Skyrme interaction

One of the objectives of this paper is to maximize the potential for detecting the sensitivity of the collision results

to the symmetry energy and its density dependence modeled according to Skyrme interactions. In the present work, we employ the SkT3 [11], and SV-bas and SV-sym34 (dubbed SV-sym from now on) [12] Skyrme interactions. In doing so, we keep in mind that the original formulation of the Skyrme potential allowed only nucleon-nucleon scattering in angular momentum s ($\ell = 0$) and p ($\ell = 1$) states [13–15], later reiterated by Vautherin and Brink [16], implying validity only for low relative momenta events. Together with the fact that parameters of the Skyrme forces are fitted to properties of finite nuclei and nuclear matter at or close to the saturation density, any extrapolation to higher densities must be treated with caution.

While the low-energy collisions covered by TDHF satisfy the low-momentum limit applicable to Skyrme forces, pBUU models of nuclear collisions at beam energies up to hundreds of MeV/nucleon where the low-momentum condition may not be fulfilled. To address this potential issue, we have adopted a compromise in evaluating proton-neutron asymmetry and symmetry energy. We consider only the asymmetry-independent terms of the energy density functional used in pBUU as a standard for collision simulations in this specific energy range. We parametrize the density dependence of the symmetry energy independently and use it as input for the simulations (see details of the procedure in Paper I and the next section).

5. The symmetry energy

We have examined the density dependence of the symmetry energy in two ways. First, the symmetry energy was computed as [17]

$$S(\rho) = \frac{1}{8}\frac{\partial^2(\mathcal{E}/\rho)}{\partial y^2}\bigg|_{\rho,y=1/2} \tag{1}$$

with $\mathcal{E}$ being the net nuclear energy density and y the ratio of Z/A. The results are shown in Fig. 1 for all the three Skyrme forces. We observe a significantly different density dependence of S predicted by the three Skyrme forces, reaching their maximum values at densities 1.5, 3.5, and 5.5 ρ_0, respectively (indicated by green arrows), and decreasing at higher densities. Interestingly, the symmetry energy becomes negative above $\rho > 3.5\ \rho_0$ for the SV-bas force, indicating a transition to neutron-only matter.

Another method of parametrization of the symmetry energy for symmetric nuclear matter is based on the Taylor expansion in terms of $\epsilon = (\rho - \rho_r)/3\rho_r$:

$$S = J + L\,\epsilon + \tfrac{1}{2}\,K_{\rm sym}\,\epsilon^2 + \tfrac{1}{6}\,Q_{\rm sym}\,\epsilon^3, \tag{2}$$

where $J \equiv S(\rho_r)$ and L, $K_{\rm sym}$, and $Q_{\rm sym}$ are the first, second, and third derivatives of the symmetry energy, usually evaluated at the saturation density $\rho_r = \rho_0$ (for details see Ref. [17]). Comparison of the results from the expansion, illustrated in Fig. 2, with the outcome of Eq. (1), in Fig. 1, indicates that the expansions start to diverge with densities increasing above the points marking the maxima of S in Fig. 1. Also, the transition to pure neutron matter predicted by Eq. (1) with the SV-bas force is not observed when retaining just the lowest terms of the expansion. The evident divergence is consistent with the limitation of the expansion to the vicinity of ρ_0 and with the low-momentum applicability of the Skyrme force. By implication, it would be unsafe to use Eq. (1) at densities higher than about (3–4) ρ_0. As discussed later, the maximum densities reached in all collisions simulated in this work are within these limits, which suggests the suitability of the Skyrme interactions, provided relative momenta stay within the limitation on account of kinematics.

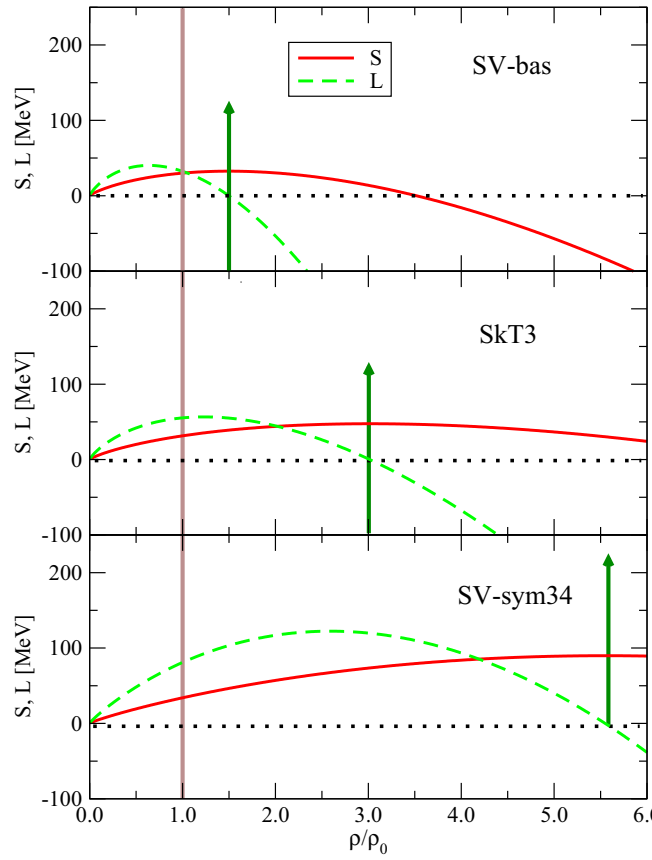

FIG. 1. The symmetry energy S and its local slope parameter L plotted vs the number density ρ in units of the saturation density ρ_0, as predicted by the SV-bas, SkT3 and SV-sym Skyrme models for the symmetric nuclear matter. The solid vertical brown line indicates the location $\rho/\rho_0 = 1.0$, and the green arrow marks the density at which the particular S maximizes. The horizontal black dotted lines guide the eye to zero, where the slope L changes sign.

III. RESULTS AND DISCUSSION

In this section, we review the main results of the calculations over the whole beam energy range. We point out similarities and differences in the pBUU and TDHF dynamics in the energy region where both approaches are expected to work. The proton-neutron asymmetries reached at high densities are examined to distinguish between impacts of the Coulomb repulsion and symmetry energy and contributions to asymmetries inherited from the initial state and coming from the high-density behavior of the symmetry energy.

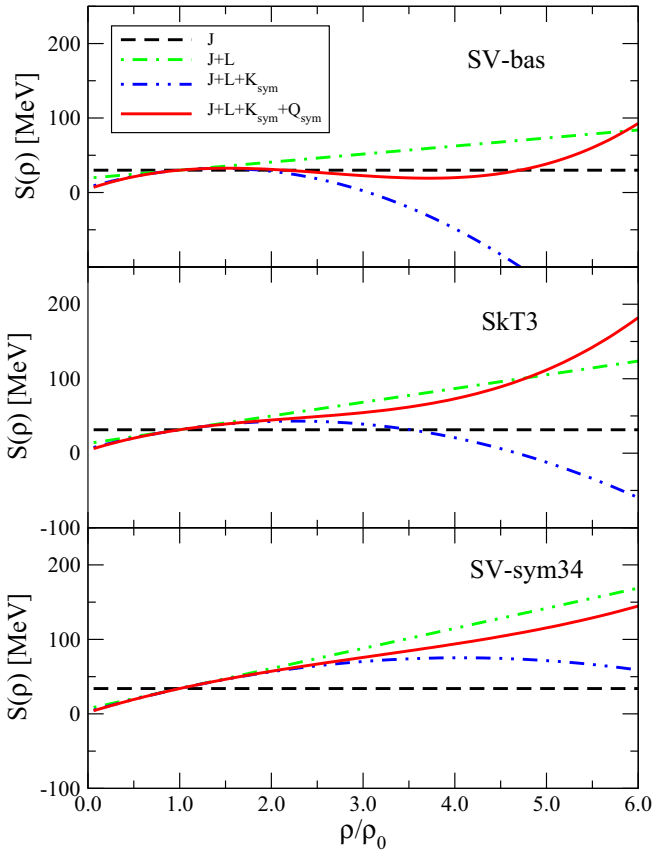

FIG. 2. Symmetry energy constructed from an increasing in size set of the lowest terms in its Taylor expansion in term of $(\rho - \rho_0)/3\rho_0$, as a function of ρ/ρ_0, as calculated using the SV-bas, SkT3, and SV-sym Skyrme parametrizations. For simplicity, the legend underscores only the dynamic coefficients for the terms, without other factors in Eq. (2).

A. Static densities

We stressed in Paper I that accurate calculation of the initial state of the collision is essential for a good-faith prediction of the proton-neutron asymmetry δ during the collision because the asymmetry is impacted at up to 50% level by the asymmetry in the initial state. We will return to this point in Sec. III B.

The top panels in Fig. 3 show the density distributions of protons and neutrons and of the total density in ^{208}Pb, as a function of distance r from the center of a nucleus, obtained by solving the static TF (in pBUU) and HF (in TDHF) equations using the SV-bas model. The proton-neutron asymmetry $\delta = [\rho_n(r) - \rho_p(r)]/[\rho_n(r) + \rho_p(r)]$ is shown in the bottom panels. In the absence of shell effects within the TF theory, the resulting densities have a smoother dependence on distance and on charge and mass numbers as compared to the HF theory. Since tunneling effects are not incorporated into the TF theory, the TF densities lack the tails falling off exponentially with distance, which is evident in the HF densities. This is particularly seen in the bottom panels, where the rise of asymmetry, marking the surface, is much sharper for TF than for HF.

To highlight next differences between the initial conditions for the collisions within the three Skyrme models, the SV-bas results are taken as a baseline. These differences in the initial state conditions for the two lead isotopes are illustrated in Figs. 4 (HF) and 5 (TF) for the proton and neutron densities (top panels) and the asymmetries (bottom panels). We observe that the radial distributions of density, whether total or for individual nucleons, vary little between the Skyrme models in the nuclear interior but vary more dramatically for values of r larger than $\approx$6 fm which is close to the experimental values of the rms radii for ^{208}Pb and ^{212}Pb, of 5.504 fm and 5.545 fm, respectively, see [18] and [19].

B. Maximum densities and the proton-neutron asymmetry

Maximal proton, neutron, and total particle number densities, as well as the proton-neutron asymmetry achievable in HIC with beam energies up to 800 MeV/nucleon, are of general interest due to sought constraints on properties of high-density matter relevant to compact astrophysical objects. We have simulated the time evolution of the collision in both the pBUU and TDHF frameworks using all three Skyrme models. We extracted the beam energy dependencies of the densities and the asymmetry $\delta = (\rho_n^{\max} - \rho_p^{\max})/(\rho_n^{\max} + \rho_p^{\max})$ as a function of the size of the colliding system and the choice of the Skyrme interaction. Notably, strictly speaking, the maximal densities for neutrons and protons may not be reached at exactly the same time or at the same location. However, we find that δ in terms of the maximal densities above gives a good overall representation of the asymmetry in the densest matter in a collision, even in systems with different projectile and target initial asymmetries.

We begin by examining the time dependence of pBUU dynamics concerning equal-density contours for individual nucleon species. Examples of the evolution of the Pb212208 collision at a beam energy of 200 MeV/nucleon are depicted in Figs. 6–8 for all three Skyrme interactions. The red contours represent protons, and blue represents neutrons. The outer dashed contours are at 0.0625 ρ_0, and the subsequent solid contours are at 0.15, 0.3, 0.45, 0.6, 0.75, and 0.9 ρ_0. It can be observed in these figures that the initial contact is followed by a build up of density in the central region, separating still-intact portions of the nuclei. Eventually, all matter flows into the region of increased density. Following the compression, the matter expands, first transversely and then in all directions, with the central density dropping. Still, the density maximizes around the system center at different times in the expanding matter.

With the symmetry energy being the only differentiating factor between the represented pBUU calculations, and total relative asymmetries being low, the evolution of total density, not directly shown in Figs. 6–8, is not much different in the three represented calculations, not only qualitatively but also quantitatively. A finer inspection, still to be discussed, shows that the softest symmetry energy, SV-bas, yields the highest compression at the system center, and the stiffest symmetry energy yields the lowest compression. These effects, however, are quite subtle. To observe more pronounced symmetry

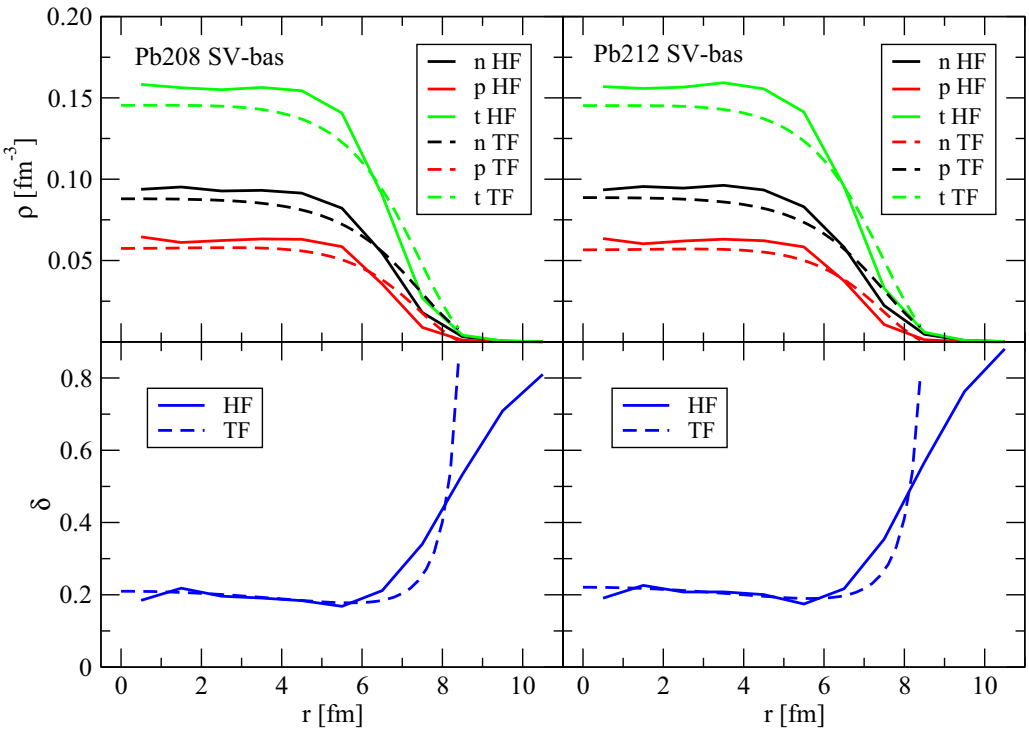

FIG. 3. Neutron (n), proton (p), and total (t) densities (top panels) and asymmetry δ (bottom panels) as functions of distance r from the center of the nucleus, for ^{208}Pb (left panels) and ^{212}Pb (right panels) from static HF and TF models following the SV-bas Skyrme force.

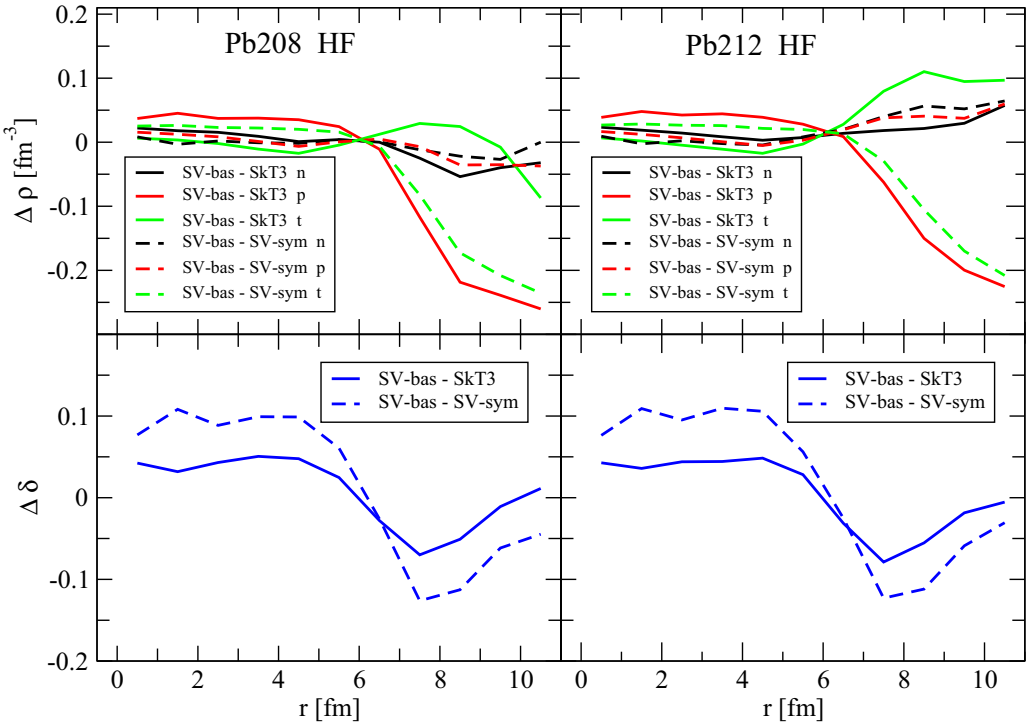

FIG. 4. Differences between densities, total and for individual nucleons (top panels), and neutron-proton asymmetries (bottom), as functions of distance r from the center of the nucleus, as predicted by HF for the SV-bas interaction model and either SkT3 or SV-sym models. Results for ^{208}Pb (left panels) and ^{212}Pb (right) are shown.

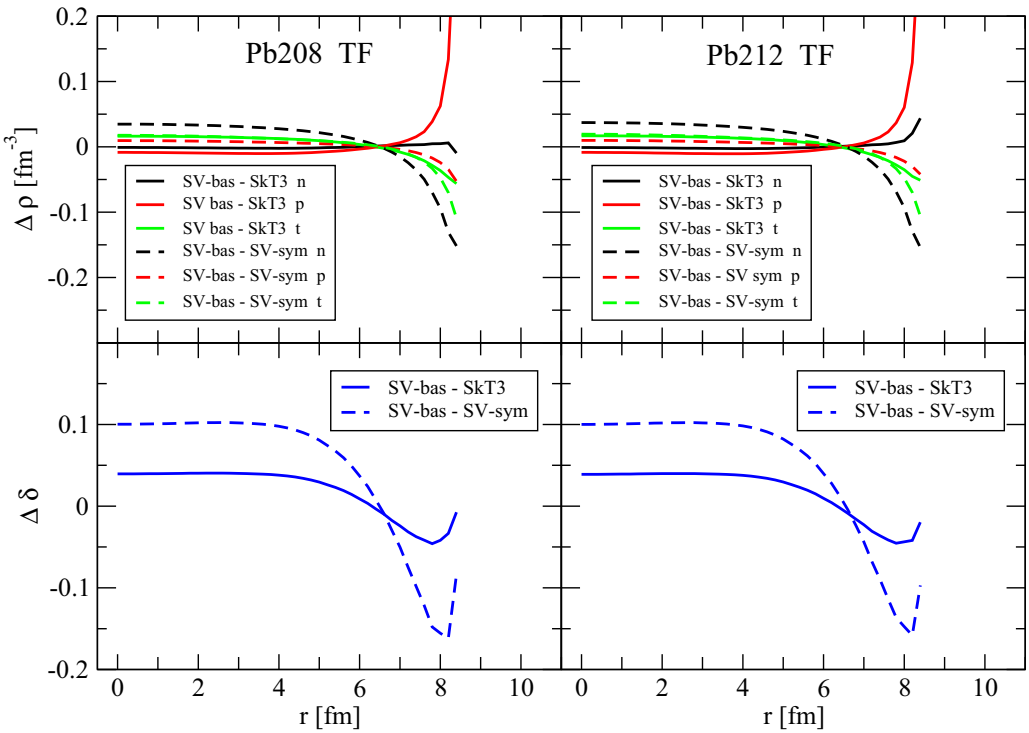

FIG. 5. The same as Fig. 4 but from TF predictions.

energy effects, neutron and proton densities must be inspected separately during the dynamics.

Looking at the contours in Figs. 6–8 in detail, neutron dominance can be seen in the tails of the density distributions as the nuclei enter their collision. That dominance generally persists at a significant level in the tails of single-particle densities further on. As the outermost proton contour, representing 0.15 ρ_0, coarsely coincides with the second outermost contour for neutrons, representing 0.3 ρ_0, until $t \approx 23\,\mathrm{fm}/c$, it is seen that the neutron density exceeds the proton density by a factor of 2 there, or $\delta \approx 0.33$. As the systems start to expand, past 23 fm/c, the density ratio in such density region drops, as again evidenced by the contours.

After the nucleonic densities first maximize around system center $t \approx 13\,\mathrm{fm}/c$ in Figs. 6–8, those densities continue to maximize around the system center. In examining the contours for neutrons and protons, we can see that those for neutrons are more tightly spaced than for protons. That difference is

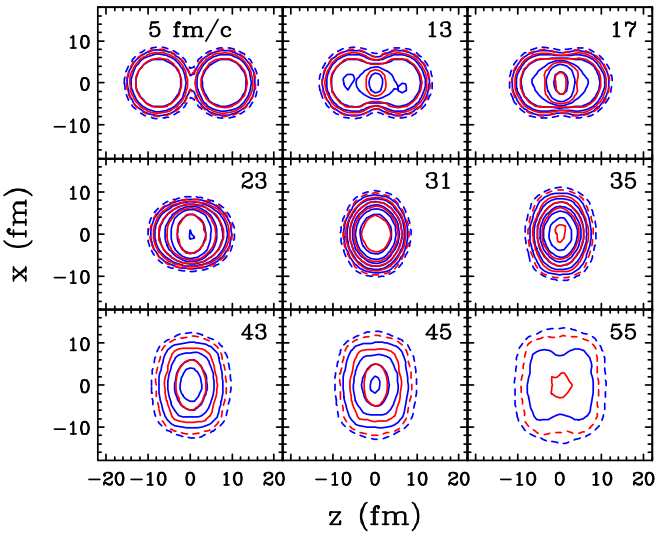

FIG. 6. Contour plots of nucleonic densities, proton (red) and neutron (blue), in the 200 MeV/nucleon ^{212}Pb + ^{208}Pb collision simulated in pBUU for the SV-bas symmetry energy. The outer dashed contours represent 0.0625 ρ_0, and the subsequent solid represents 0.15, 0.3, 0.45, 0.6, 0.75, and 0.9 ρ_0.

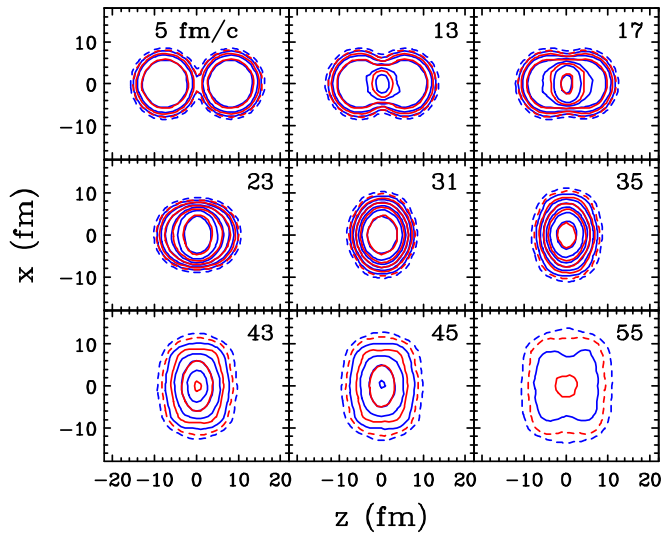

FIG. 7. The same as Fig. 6, but for the SkT3 symmetry energy.

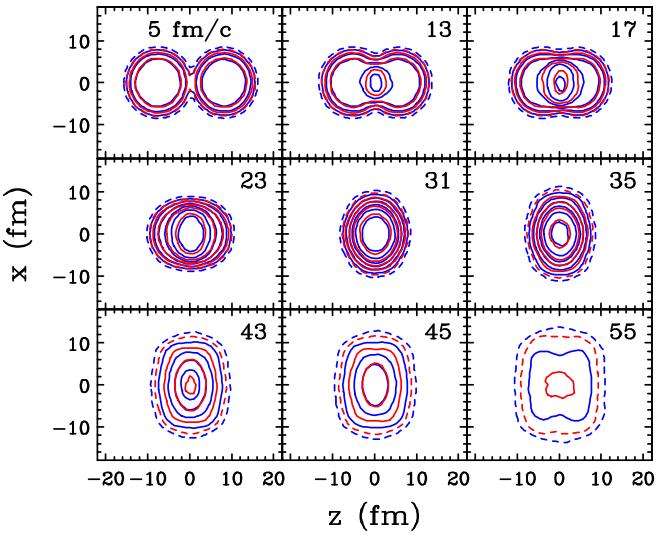

FIG. 8. The same as Fig. 6, but for the SV-sym symmetry energy.

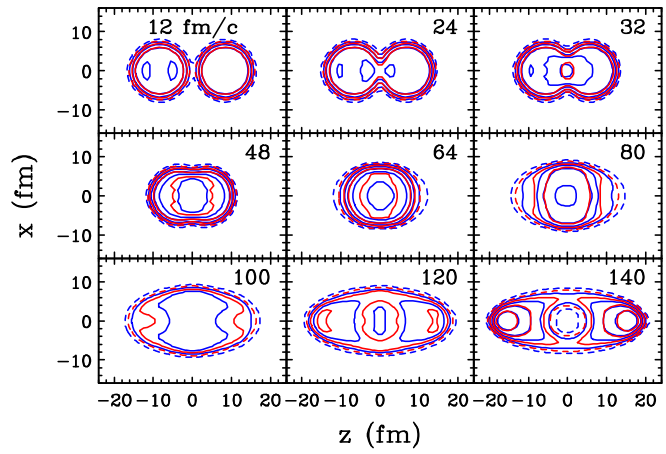

FIG. 9. Contour plots of nucleonic densities, proton (red) and neutron (blue), in the 40 MeV/nucleon ^{212}Pb + ^{208}Pb collision simulated in TDHF for the SV-bas interaction.

primarily due to the overall neutron dominance, the neutron number in the system being larger than proton. When the neutron and proton contours coincide around the maximal nucleonic densities at $t \approx 23\,\mathrm{fm}/c$ in Figs. 6–8, close to the maximum compression for total density, the index for the neutron contour is by 2 ahead of that for the proton. The latter means that the isosurface for $0.9\,\rho_0$ neutron density roughly coincides with the isosurface for $0.6\,\rho_0$ proton density, yielding $\delta \approx 0.20$ there, this close to the system asymmetry.

When we compare results for different symmetry energies, Figs. 6–8, we begin to see differences between the evolutions they drive. Thus, at $t = 31\,\mathrm{fm}/c$, the $0.6\,\rho_0$ p-isosurface is inside the $0.9\,\rho_0$ n-isosurface for SV-bas in Fig. 6 and the reverse is true for SV-sym in Fig. 8. For SkT3 symmetry energy in Fig. 7, these isosurfaces most tightly coincide among the three evolutions. These features point to the highest asymmetries δ for the SV-bas evolution in the high-density region, lowest for SV-sym, and intermediate for SkT3.

Besides the differences in asymmetry around the maximal nucleonic densities at maximum compression, there are differences in how the densities for protons and neutrons rise and drop for the different symmetry energies, as may be again evident from the density contours. While the relative asymmetry δ generally decreases with time for SV-sym at the highest densities around the maximum compression, time frames $t = 17\,\mathrm{fm}/c$ to $t = 35\,\mathrm{fm}/c$ in Fig. 6, δ increases between those time frames for SV-bas in Fig. 8. The last surprising result can be tied to the fact that the potential part of the symmetry energy is dropping with net density in the vicinity of $\rho/\rho_0 \approx 1.5$, as the kinetic part rises and the combination of the two is approximately constant there in Fig. 1. Strengthening the Coulomb field with compression helps increase the asymmetry, too. Even for SkT3, some muted increase in the relative asymmetry at maximal densities is observed with time.

Next, the time dependence of TDHF dynamics in terms of contour plots of nucleonic densities in the Pb212208 collision at beam energy 40 MeV/nucleon in Figs. 9–11 for the three Skyrme interactions is shown. TDHF validity is conditioned on the Pauli-principle suppression of nucleon-nucleon collisions. As beam energy increases, the role of the Pauli principle gradually weakens, allowing for more collisions. The beam energy is about the upper limit when one still learns about the collision of the heavy nuclei while relying on TDHF.

In Figs. 9–11, we can see an impact of shell effects on the density distributions. They are visible in the early $t = 12\,\mathrm{fm}/c$ and $24\,\mathrm{fm}/c$ distributions for SV-bas and SkT3 interactions, and they still have some impact on the higher density area for all three interactions at $t = 32\,\mathrm{fm}/c$. Without nucleon-nucleon collisions, the higher density region is much less localized than at the higher energies in pBUU. The constituents of the two nuclei largely persist in their primary motion along the beam axis, and there is very little transverse expansion like in pBUU at 200 MeV/nucleon. Still, the nucleonic densities at any one time are not a simple superposition of shifted densities in the original nuclei; this is on account of the interaction impact cast in the semiclassical limit in the phase-space avoidance of the matter from the two nuclei governed then by the single-particle Liouville or Vlasov equations [20,21]. With this, the distributions are more spread out during the nuclear

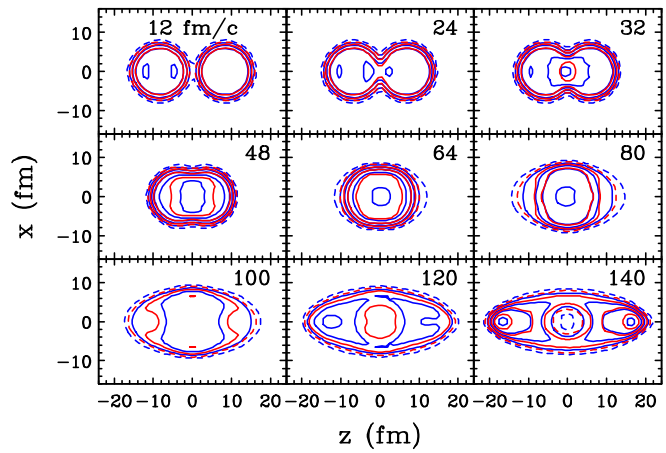

FIG. 10. The same as Fig. 9, but for the SkT3 symmetry energy.

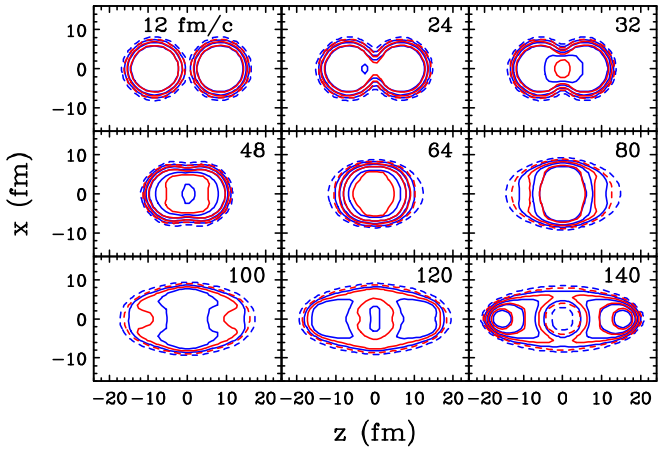

FIG. 11. The same as Fig. 9, but for the SV-sym symmetry energy.

overlap than for either individual nuclei, and the maximal densities are lower than for the simple superposition.

Around the time frame $t = 64\,\mathrm{fm}/c$ in Figs. 9–11, the system may seem fused. However, the system is not equilibrated. The preference for motion along the beam axis persists, and the density distributions of the two original nuclei gradually emerge after penetrating each other. The emerging fragments are distorted and somewhat slowed down in the center of mass compared to the original nuclei, but their total nucleonic content is nearly unchanged. This outcome has no noticeable dependence on the symmetry energy.

We next turn to the beam energy dependence of maximal nucleonic densities reached in the head-on PB212208 collisions and of asymmetries for those densities. The results for pBUU are represented in Figs. 12 and 13 and those for TDHF—in Table I. In each case, the results can be seen for calculations with and without Coulomb interactions. Moreover, the results can be found for the three Skyrme interactions, for pBUU in Fig. 12 and for TDHF in Table I. Finally, in Fig. 13 we provide results from the pBUU calculations in the Vlasov approximation for the SV-bas symmetry energy.

In Table I and the figures, a strong impact of Coulomb interactions on the reached asymmetries and the total density at a given beam energy can be seen. Compared to the no-Coulomb case, the Coulomb interactions increase the asymmetries by (50–80)% and decrease the total density by ≈10%. The impacts of the Coulomb interactions are more robust than those of varying the stiffness of symmetry energy within its general uncertainty range. We stress again [2] that thorough modeling of the Coulomb effects is needed to pin down the stiffness of the symmetry energy from collision outcomes. For all energies, the stiffest symmetry energy, SV-sym, gives rise to the lowest asymmetries for the maximal densities and the softest, SV-bas, to the highest. The impact of the symmetry-energy stiffness is nominally reversed on the total density but is relatively marginal.

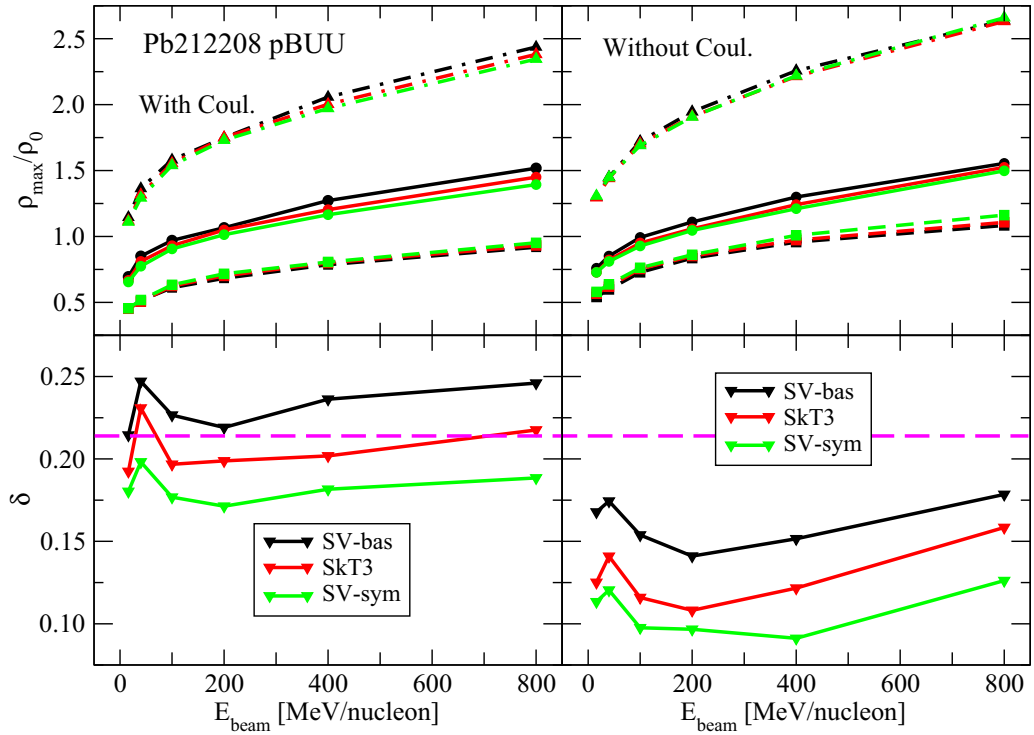

FIG. 12. Top panels: Evolution of normalized maximal proton (red), neutron (black), and total nucleon (green) number density with increasing beam energy in the pBUU simulation, as predicted with the SV-bas, SkT3, and SV-sym Skyrme symmetry energies. The solid (dashed) connecting lines mark the neutron (proton) densities, and the dashed-dot lines mark the total densities. Bottom panels: Corresponding proton-neutron asymmetries δ. The horizontal magenta dashed line marks the initial asymmetry of the projectile and target. Left/right panels: Results obtained with/without Coulomb interactions.

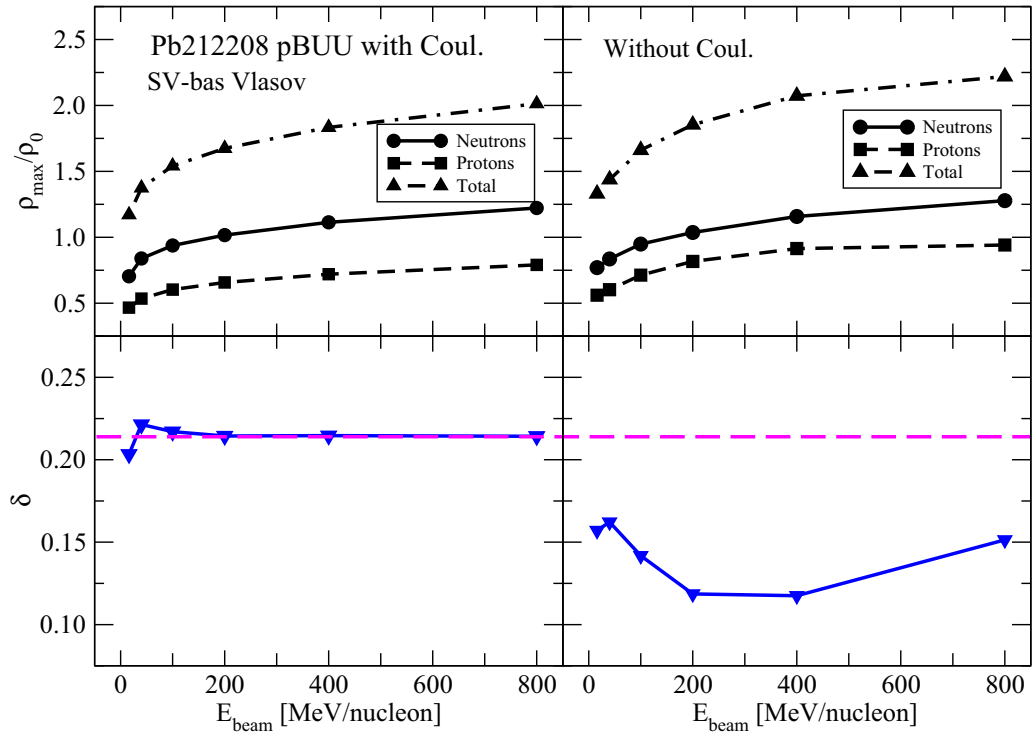

FIG. 13. The same content as in Fig. 12, but now for calculations in the Vlasov approximation with SV-bas Skyrme symmetry energy only.

In comparing the SV-bas symmetry energy results in Figs. 12 and 13, we can observe the impact of elementary collisions on the nucleonic densities. The collisions help to trap nucleons in the central region of the nuclear collision, allowing the total density to accumulate there. However, while the nucleons persist in the central region longer, the asymmetry favored by the dropping potential symmetry energy with density, for the higher densities, has time to grow at the expense of the exterior, leading to an increase in the asymmetry for higher beam energies compared to the Vlasov case. In comparing the results for SV-bas in Fig. 13 and Table I, we can observe the impact of the shell effects that lead to a ≈15% increase in the asymmmetry for maximal densities in TDGF, as compared to pBUU.

TABLE I. Maximum densities of different indicated species, in units of normal density, and asymmetries δ as predicted in the HF model with the SV-bas, SkT3, and SV-sym Skyrme interactions in the Pb212208 collisions at beam energies of 10 and 40 MeV/nucleon. Results with and without (nC) the Coulomb interaction are shown. Data for SV-bas and SV-sym Skyrme interactions have been taken from [2], for completeness.

		10	40	10 nC	40 nC
SV-bas	p	0.429	0.478	0.532	0.592
	n	0.714	0.827	0.760	0.849
	p+n	1.144	1.305	1.292	1.441
	δ	0.229	0.267	0.176	0.178
SKT3	p	0.434	0.499	0.553	0.607
	n	0.702	0.811	0.744	0.838
	p+n	1.136	1.310	1.297	1.445
	δ	0.236	0.238	0.148	0.160
SV-sym	p	0.464	0.511	0.563	0.590
	n	0.675	0.758	0.734	0.772
	p+n	1.139	1.269	1.297	1.362
	δ	0.185	0.195	0.132	0.134

We complement the findings so far with the profiles of neutron-proton asymmetry, $\rho_n(\mathbf{r}) - \rho_p(\mathbf{r})$, in a direction perpendicular to the beam axis from the system center at different times, for SkT3, in the pBUU dynamics at 200 MeV/nucleon in Fig. 14 and in the TDHF dynamics at 40 MeV/nucleon in Fig. 15. Similar results for SV-bas and SV-sym were shown in Ref. [2]. The asymmetry results are shown for simulations with included Coulomb interactions, left panels, and with those interactions excluded, right panels. Separately shown are the profiles on the top panels when the central asymmetry increases with time and when the central asymmetry generally decreases on the bottom panels. In comparing the results with and without the Coulomb interactions, we can observe an increase in the absolute asymmetry at the system center due to these interactions. Simultaneously, however, we can see that this increase is somewhat limited in the transverse spatial and temporal extensions. In TDHF, there are changes in the progress of the collision in the absence of Coulomb interactions, as disengagement of the original nuclei in the later stages of the collision, or fission, stalls. Comparing the pBUU results for different symmetry energies, here in Fig. 14 and Figs. 6 and 7 of Ref. [2], we can see that, while a softer symmetry energy density dependence leads to higher $\rho_n - \rho_p$ values around the highest total densities, this comes at the cost of an increasingly limited span of the highest asymmetry densities both in space and time.

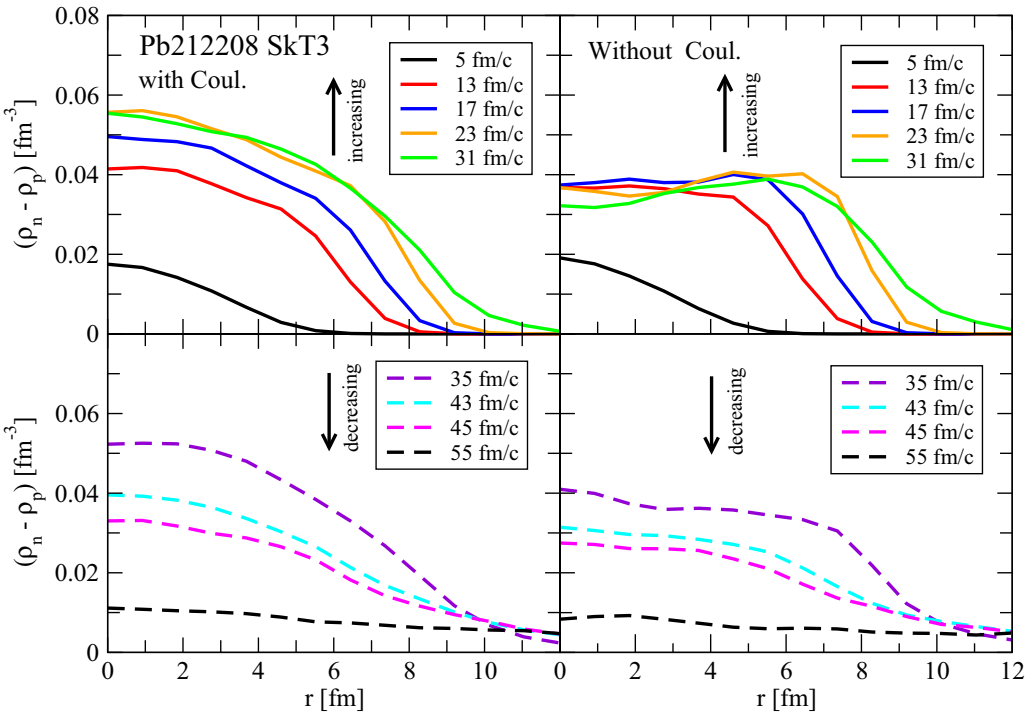

FIG. 14. Comparison of neutron and proton densities, obtained in the pBUU transport model with SkT3 symmetry energy vs. distance to the symmetry axis in the transverse direction, from the center of the collision, for the Pb212208 system at the beam energy of 200 MeV/nucleon. The time intervals represented in the top panels are 5–31 fm/c (solid lines) and in the bottom panels 35–55 fm/c (dashed lines), from the first contact of the nuclei. The arrows indicate increasing and decreasing isospin differences throughout the collision. The left (right) panels show results with (without) Coulomb interaction.

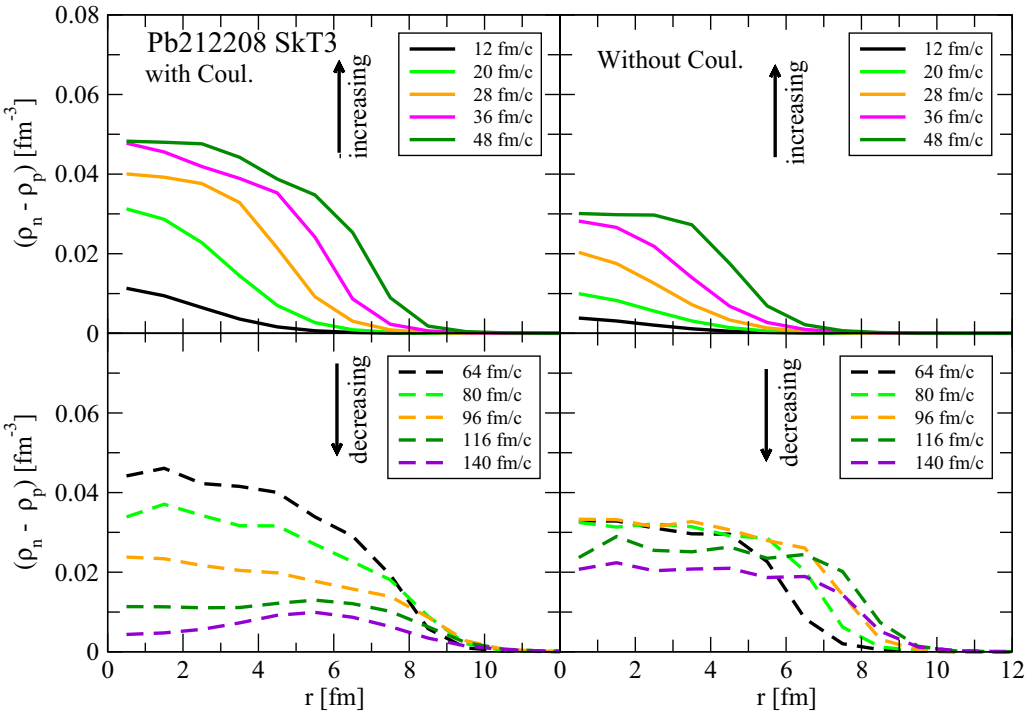

FIG. 15. The same as Fig. 14, but in the TDHF formalism at the beam energy of 40 MeV/nucleon. See text for comments on the bottom left panel.

IV. CONCLUSIONS AND OUTLOOK

We have extended our investigation of the impact of Coulomb interactions, in addition to the variants of symmetry energy density dependence, on the maximal densities and on related proton-neutron asymmetries in the $^{212}\mathrm{Pb} + ^{208}\mathrm{Pb}$ collision. In this system, the Coulomb interactions are the strongest compared to the asymmetric systems we studied before, $^{54}\mathrm{Ca} + ^{48}\mathrm{Ca}$ and $^{132}\mathrm{Sn} + ^{124}\mathrm{Sn}$. Also, for the Pb system, we presented results obtained with the SkT3 symmetry energy with the slope parameter L intermediate for the SV-bas and SV-sym energies included before. Moreover, we added details for all symmetry-energy versions, included contour plots and provided extra insights into the TDHF results.

To summarize our quest for maximum particle number density and proton-neutron asymmetry in HIC with a beam energy below 800 MeV/nucleon in the present work, Paper I, and Ref. [2], we find that

(i) The highest total densities predicted at $E_{\mathrm{beam}} = 800\,\mathrm{MeV/nucleon}$ are of the order of $\approx 2.5\,\rho_0$ ($\rho_0 = 0.16\,\mathrm{fm}^{-3}$).

(ii) The proton-neutron asymmetry δ at maximum density strongly depends on the asymmetry in the initial state of the collision and on Coulomb interactions. In most cases, it does not exceed the asymmetry in the initial state of the collision at all beam energies and generally decreases in the reaction. Even when higher asymmetries are reached for models with a softer symmetry energy density dependence, this occurs at the cost of reduced persistence of those asymmetries as a function of space and time.

(iii) Coulomb effects mask pure nuclear effects to a degree that cannot be neglected. These effects complicate relating properties of the high-density matter created in heavy-ion reactions and the electrically neutral matter in compact astrophysical objects.

ACKNOWLEDGMENT

This work was supported by the U.S. Department of Energy Office of Science under Grant No. DE-SC0019209.

[1] J. R. Stone, P. Danielewicz, and Y. Iwata, Phys. Rev. C **96**, 014612 (2017).
[2] J. R. Stone, P. Danielewicz, and Y. Iwata, Phys. Lett. B **826**, 136915 (2022).
[3] P. Danielewicz, Nucl. Phys. A **673**, 375 (2000).
[4] J. A. Maruhn, P.-G. Reinhard, P. D. Stevenson, and A. S. Umar, Comput. Phys. Commun. **185**, 2195 (2014).
[5] P. Danielewicz and G. Bertsch, Nucl. Phys. A **533**, 712 (1991).
[6] Y. Iwata, T. Otsuka, J. A. Maruhn, and N. Itagaki, Phys. Rev. Lett. **104**, 252501 (2010).
[7] J. Aichelin, Phys. Rep. **202**, 233 (1991).
[8] A. Ono, P. Danielewicz, W. A. Friedman, W. G. Lynch, and M. B. Tsang, Phys. Rev. C **70**, 041604(R) (2004).
[9] J. F. OHanlon, *A Users Guide to Vacuum Technology* (Wiley, New York, 2003).
[10] K. Malek and M.-O. Coppens, J. Chem. Phys. **119**, 2801 (2003).
[11] F. Tondeur, M. Brack, M. Farine, and J. Pearson, Nucl. Phys. A **420**, 297 (1984).
[12] P. Klüpfel, P.-G. Reinhard, T. J. Bürvenich, and J. A. Maruhn, Phys. Rev. C **79**, 034310 (2009).
[13] T. H. R. Skyrme, Philos. Mag. **1**, 1043 (1956).
[14] J. S. Bell and T. H. R. Skyrme, Philos. Mag. **1**, 1055 (1956).
[15] T. H. R. Skyrme, Nucl. Phys. **9**, 615 (1958-1959).
[16] D. Vautherin and D. M. Brink, Phys. Rev. C **5**, 626 (1972).
[17] M. Dutra, O. Lourenço, J. S. S. Martins, A. Delfino, J. R. Stone, and P. D. Stevenson, Phys. Rev. C **85**, 035201 (2012).
[18] I. Angeli and K. Marinova, At. Data Nucl. Data Tables **99**, 69 (2013).
[19] I. Angeli and K. P. Marinova, J. Phys. G: Nucl. Part. Phys. 42, 055108 (2015).
[20] H. Tang, C. Dasso, H. Esbensen, R. Broglia, and A. Winther, Phys. Lett. B **101**, 10 (1981).
[21] G. Bertsch and S. D. Gupta, Phys. Rep. **160**, 189 (1988).